Simulation of biomass char gasification in a downdraft reactor for syngas production

Augustina Ephraim, Victor Pozzobon, Olivier Louisnard, Doan Pham Minh, Ange Nzihou, Patrick Sharrock

Simulation of Biomass Char Gasification in a Downdraft Reactor for Syngas Production

Augustina Ephraim, Victor Pozzobon, Olivier Louisnard, Doan Pham Minh, Ange Nzihou, and Patrick Sharrock
Université de Toulouse, Mines Albi, UMR CNRS 5302, Centre RAPSODEE, Campus Jarlard, F-81013 Albi cedex 09, France

A steady state, one-dimensional computational fluid dynamics model of wood char gasification in a downdraft reactor is presented. The model is not only based on reaction kinetics and fluid flow in the porous char bed but also on equations of heat and mass conservation. An original OpenFOAM solver is used to simulate the model and the results are found to be in good agreement with published experimental data. Next, a sensitivity analysis is performed to study the influence of reactor inlet temperature and gas composition on char conversion, bed temperature profile and syngas composition. In addition, the evolution of the complex reaction mechanisms involved in mixed atmosphere gasification is investigated, and the most suitable operating parameters for controlling syngas composition are evaluated. Our simulation results provide essential knowledge for optimizing the design and operation of downdraft gasifiers to produce syn-gas that meets the requirements of various biofuel applications.
Keywords: biomass waste, gasification, syngas, model simulation, downdraft reactor, OpenFOAM

Introduction

As global energy demand is projected to rise by nearly 56% to 865 EJ between 2010 and 2040, syngas will become increasingly important for electric power generation, process heat and liquid fuel production.[1] Syngas is a mixture of hydrogen (H_2) and carbon monoxide (CO) produced from the gasification of carbonaceous feedstock. As biomass is the only renewable carbon-based energy source, syngas produced from waste biomass (biosyngas) will be a key-intermediate in the future production of renewable fuels to meet national renewable energy and global carbon-dioxide-emission reduction targets.[2] Examples of waste biomass materials include residues from forest and wood processing industries such as wood chips, saw dust and bark, and agricultural residues such as straw, bagasse, and husk.[3]

Pyrolysis is the thermal conversion of biomass under inert or oxygen-deficient atmosphere at temperatures between 500 and 800℃. The three primary products of pyrolysis are bio-oil, char and gas. At high temperatures (>800℃), the char produced from pyrolysis can be gasified with gasification agents such as steam (H_2O), carbon-dioxide (CO_2), and oxygen (O_2) in air to produce syngas. The most important industrial applications of syngas, so far practiced commercially or under research studies, can be summarized as follows[4,5]:

1. Electricity production in steam cycles, gas engines, turbines (combined cycle), and fuel cells,

2. Chemical synthesis of hydrogen (for refineries), Synthetic Natural Gas and ammonia (mainly for fertilizer production),

3. Transport fuel synthesis from Gas-to-Liquids processes including Fischer–Tropsch (FT) diesel and methanol/dimethyl ether.

The choice of syngas end-use mainly depends on its composition (H_2/CO ratio) as shown in Table 1.[6] Several operating parameters influence the composition of syngas, the most important of which are the gasification agent, reactor temperature, biomass properties and the use of catalysts in the gasification process.[7–9] As a result of the highly heterogeneous nature of waste biomass feedstock, the prediction of syngas H_2/CO ratio from the physical and chemical properties of biomass char has proven to be difficult.[10] Consequently, recent research works have focused on studying the influence of temperature, gasification agents and catalysts on syngas composition to manipulate the syngas ratio and better control the gasification process.[6,10–15] This ensures that the biomass feedstock has a lesser impact on the syngas produced and thus offers greater fuel flexibility to meet the requirements of the desired syngas application.[6]

In view of engineering design and process optimization of a biomass gasifier for syngas production, an extensive investigation of the plant behavior depending on various operating parameters is required.[16] Performing experiments at large scales are often problematic mainly due to their associated safety risks and high costs. Hence, developing a mathematical model that gives a good representation of the complex chemical and physical phenomena occurring in the gasifier is desirable as it allows fewer and better experiments to be performed with minimal

Table 1. Examples of Syngas End-Uses and Their Approximate H_2/CO Ratio Requirements[6]

Syngas End-Use	H_2/CO Ratio
Solid oxide fuel cells (SOFC)	4.0–6.0
Gas turbine combustion	2.5–4.0
Fischer–Tropsch (diesel fuels)	1.5–3.0
Fischer–Tropsch—Fe and Co—based catalyst process	0.5–1.5

temporal and financial costs. In addition, a simulation model enables prediction of the evolution of these complex phenomena which is essential for optimizing the reactor design and its operating conditions.[17] For models of biomass char gasification, the vast majority of those presently found in literature are kinetic models obtained from the study of char reactivity in different atmospheres and temperature ranges,[18–22] disregarding diffusive and convective heat and mass transfer, and thus neglecting temperature and composition gradients in the sample. Conversely, computational fluid dynamics (CFD) modeling techniques applied to biomass char gasification are scarce and are currently restricted to either coal gasification or biomass combustion/gasification in entrained flow reactors.[17] CFD programs allow the coupling of fluid flow, heat and mass transfer to chemical reactions and other related phenomena, by numerically solving the set of governing conservation equations: mass, heat, and momentum.[23] To the best of our knowledge, the most recent experimentally validated CFD model in literature on char gasification is that of Teixeira et al.[24] who developed a steady state, one-dimensional (1-D) model of wood char gasification in a downdraft reactor.
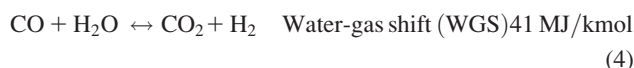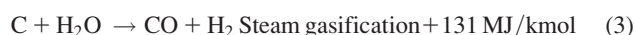
In this article, modifications are made to the latter CFD model in an attempt to improve its prediction of syngas composition. An original in-house built solver based on Open-FOAM is used to simulate the model, and the results are validated against the experimental data of Teixeira et al.[24] OpenFOAM is an open source CFD software package which offers users complete freedom to customize and extend its existing functionality. OpenFOAM's capacity to solve complex CFD problems is comparable to that of reputed powerful close sourced software such as ANSYS Fluent. Although OpenFOAM has a large user community across most areas of engineering and science, it has been scarcely used for simulating biomass gasification. The only biomass gasification solver found in literature is biomassGasificationFOAM which was developed by Kwiatkowski et al.[25] to simulate the pyrolysis and gasification of a single biomass particle. Thus until now, no OpenFOAM solver has been developed to simulate the gasification of biomass at the reactor scale in a downdraft fixed bed gasifier. Next in this article, a sensitivity analysis is performed to study the influence of temperature and a mixed atmosphere (O_2, H_2O, CO) on char conversion, bed temperature profile and H_2 and CO production (H_2/CO ratio). This sensitivity analysis will enable clarification of the complex reaction mechanisms involved in mixed atmosphere gasification, and an evaluation of the most suitable operating parameter(s) for optimizing syngas composition, to meet the requirements of the desired industrial application.

Modeling Approach

A schematic view of a downdraft reactor is shown in Figure 1a. The biomass particles are fed at the top of the reactor and slowly flow to the bottom where the residual ash is withdrawn. The gasification agents are injected through the sides of the reactor. During their downward flow, the biomass particles undergo the following main processes: drying, pyrolysis, combustion and reduction. Finally, the produced gas is withdrawn from the bottom of the reactor.

Our work focuses on modeling the gasification of char produced from the pyrolysis of wood biomass by considering reactions of char with the gasification agents, air (O_2 + N_2), steam (H_2O) and carbon dioxide (CO_2). The reactions considered in this model and their associated heats of reaction at 25°C are

$$C + O_2 \rightarrow CO_2 \quad \text{Combustion} \quad -394\,\text{MJ/kmol} \quad (1)$$

$$C + CO_2 \rightarrow 2CO \quad \text{Boudouard} \quad +172\,\text{MJ/kmol} \quad (2)$$

$$C + H_2O \rightarrow CO + H_2 \, \text{Steam gasification} +131\,\text{MJ/kmol} \quad (3)$$

$$CO + H_2O \leftrightarrow CO_2 + H_2 \quad \text{Water-gas shift (WGS)} 41\,\text{MJ/kmol} \quad (4)$$

where the N_2 in air has been assumed to remain inert.

Figure 1b shows the char bed in the gasification zone of the reactor in which the equations of mass, heat and momentum are solved. The boundary conditions for these equations are applied at the bed inlet and outlet ($z = 0$ and $z = $ H, respectively).

Assumptions

The following assumptions were made to model the gasification of wood char in the downdraft reactor:

1. Steady-state operation as most industrial downdraft gasifiers operate for long periods with few interruptions and the feed and withdrawal rates of the solid and gas phases have relatively low fluctuations.

2. Laminar flow regime for the gas phase due to the low velocities usually encountered in fixed bed reactors.

3. Ideal gas mixture as most downdraft gasifiers operate at atmospheric pressure.

4. Char bed is a homogeneous porous media so that all variables are assumed continuous in space and time.

5. At the pore scale, there is no heat transfer resistance between the solid and the gas phases. This assumption is based on the experimental findings of Van de Steene et al.[26]
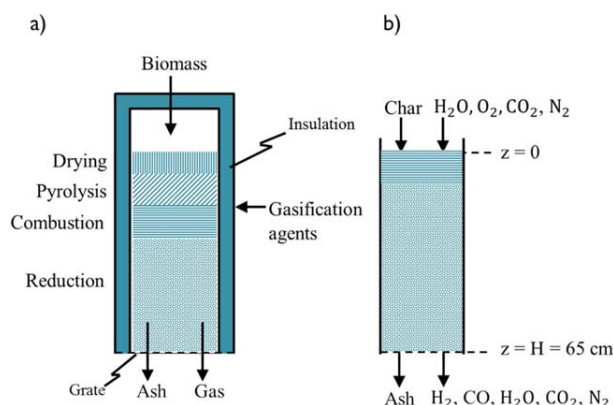

Figure 1. (a) Schematic view of a downdraft reactor and (b) Model representation of the char gasification zone.

[Color figure can be viewed in the online issue, which is available at wileyonlinelibrary.com.]

The complex medium can therefore be represented with a single temperature field ($T_g = T_c = T$).

6. Heat transfer by radiation is neglected due to the relatively large flows of gas and solid which renders convective and conductive heat transfer predominant.

7. Constant bed porosity, tortuosity and particle diameter are assumed along the char bed as the evolution of these parameters with char conversion is very difficult to determine.

Mathematical equations and boundary conditions

Continuity Equation for Gas Phase Coupled to Momentum Balance (Darcy's Law). The continuity equation for the gas phase is written as

$$\nabla \cdot (U_g C_g) = \sum_{j=1}^{6} r_j \tag{5}$$

where U_g is the superficial gas velocity, C_g is the total gas concentration and r_j is the mass source of gas species j, where j belongs to CO, CO_2, H_2O, O_2, H_2.

By considering the gas as an ideal mixture, C_g can be expressed as a function of bed pressure P, and temperature T, by

$$C_g = \frac{P}{RT} \tag{6}$$

where R is the universal gas constant.

As with several other fixed bed models,[27–29] Darcy's law is used to describe the average flow of gas through the porous char bed as

$$U_g = -\frac{K}{\mu} \nabla P \tag{7}$$

where K is the bed permeability and μ is the gas viscosity.

Darcy's law can be coupled to the continuity equation by substituting Eqs. 6 and 7 into Eq. 5 to finally give

$$\nabla \cdot \left(-\frac{P}{RT} \frac{K}{\mu} \nabla P \right) = \sum_{j=1}^{6} r_j \tag{8}$$

Mass Balance Equation for Each Gas Phase Species. The mass balance for each chemical species j in the gas phase is given by

$$\nabla \cdot (U_g C_{g,j}) = \nabla \cdot (D^*_{j,N_2} \nabla C_{g,j}) + r_j \tag{9}$$

The left-hand side of Eq. 9 represents the contribution of the convective mass transfer and the first term on the right-hand side represents diffusive transfers. Here we have assumed that since N_2 is the dominant gas in the gas phase, the effective diffusion coefficient of species j in the gas phase is equivalent to the effective diffusion coefficient D^*_{j,N_2} of species j in pure N_2. This effective diffusion coefficient is a function of the bed porosity ε, and the bed tortuosity τ[30] and the bulk diffusion coefficient between species j and N_2

$$D^*_{j,N_2} = \frac{\varepsilon}{\tau} D_{j,N_2} \tag{10}$$

The dependence of the bulk diffusion coefficient D_{j,N_2} on temperature and pressure is expressed according to the Chapaman–Enskog formula

Table 2. Expression for Diffusion Coefficient of Gaseous Species as a Function of Temperature and Pressure (Chapaman–Enskog formula)[31]

Chemical Species j	Diffusion Coefficient D_{j,N_2} (m²/s)
N_2	$1.39 \cdot 10^{-4} \cdot \left(\frac{1.013 \cdot 10^5}{P} \right) \cdot \left(\frac{T}{1173} \right)^{3/2}$
CO_2	$1.13 \cdot 10^{-4} \cdot \left(\frac{1.013 \cdot 10^5}{P} \right) \cdot \left(\frac{T}{1173} \right)^{3/2}$
H_2O	$2.11 \cdot 10^{-4} \cdot \left(\frac{1.013 \cdot 10^5}{P} \right) \cdot \left(\frac{T}{1173} \right)^{3/2}$
CO	$1.40 \cdot 10^{-4} \cdot \left(\frac{1.013 \cdot 10^5}{P} \right) \cdot \left(\frac{T}{1173} \right)^{3/2}$
H_2	$5.11 \cdot 10^{-4} \cdot \left(\frac{1.013 \cdot 10^5}{P} \right) \cdot \left(\frac{T}{1173} \right)^{3/2}$
O_2	$1.43 \cdot 10^{-4} \cdot \left(\frac{1.013 \cdot 10^5}{P} \right) \cdot \left(\frac{T}{1173} \right)^{3/2}$

$$D_{j,N_2} = D_{j,N_2}(T_{ref}, P_{ref}) \left(\frac{P_{ref}}{P} \right) \left(\frac{T}{T_{ref}} \right)^{3/2} \tag{11}$$

where $D_{j,N_2}(T_{ref}, P_{ref})$ is the diffusivity of species j in nitrogen (N_2) gas solvent under reference conditions. Table 2 lists the expression for the diffusion coefficient for each gaseous species j.

The bed tortuosity is approximated by[32]

$$\tau = 1 - 0.41\ln(\varepsilon) \tag{12}$$

Finally, the last term r_j in the RHS of Eq. 9 is the production rate of species j, and will be detailed hereafter.

Mass Balance Equation for the Solid Phase (Char). The mass balance equation for the solid phase is given by

$$\nabla \cdot (U_c C_c) = r_c \tag{13}$$

where U_c and C_c are the velocity and concentration of char, respectively, and r_c is the sink term for the consumption of char by the chemical reactions.

The velocity of char in a downdraft reactor can decrease significantly as a result of bed compaction. Bed compaction is a consequence of the reduction of particle size due to carbon conversion and various mechanical phenomena such as fragmentation and particle rearrangement.[33] Equation 13 can be coupled to the char bed compaction equation which expresses the solid phase velocity as a function of char conversion X

$$U_c(X) = U_{c,0} f(X) \tag{14}$$

where $f(X)$ is an empirical function developed by Teixeira et al.[24] and determined for wood char chips

$$f(X) = -1.03 \cdot 10^{-4} X^2 + 4.25 \cdot 10^{-4} X + 1 \tag{15}$$

The conversion of char is calculated from the molar flow rates of the gaseous carbon species produced (CO and CO_2)

$$X = \frac{\dot{n}_c|_{z=0} - \dot{n}_c}{\dot{n}_c|_{z=0}} = \frac{\dot{n}_{CO} + \dot{n}_{CO_2} - \dot{n}_{CO_2}|_{z=0} - \dot{n}_{CO}|_{z=0}}{\dot{n}_c|_{z=0}} \tag{16}$$

Reaction Kinetics. The reaction rates for the heterogeneous reactions v_i (Eqs. 1–3) are determined by

$$v_i = \omega_i C_{c,0} \tag{17}$$

where $C_{c,0}$ is the initial concentration of char and the notation ω_i denotes the char conversion rate for each heterogeneous reaction (1)–(3). These char conversion rates have been correlated by Teixeira and coworkers to the experimental parameters, temperature T and partial pressure of the reactant gas P_j

Table 3. Coefficient Values of the Functions for the Three Heterogeneous Reactions[34]

Reaction	Steam Gasification	Boudouard	Oxidation
a	-2.38×10^1	-3.30×10^1	-7.83
b	2.92×10^{-2}	4.18×10^{-2}	8.65×10^{-3}
c	2.63	2.86	2.32×10^1
d	3.72×10^2	6.01×10^2	-2.89×10^2
e	-4.33	-6.42	-3.52
f	3.32×10^{-6}	1.48×10^{-8}	1.13×10^{-10}
g	-1.02×10^{-5}	-1.45×10^{-5}	-3.12×10^{-6}
h	-2.88	-2.90	-6.59×10^1
i	-4.08×10^{-1}	-5.86×10^{-1}	2.85×10^4
j	3.39×10^{-3}	4.86×10^{-3}	3.78
k	-2.59×10^{-9}	-1.12×10^{-11}	-4.95×10^{-3}
l	8.38×10^{-7}	1.34×10^2	-9.54×10^{-2}
m	1.19×10^2	-2.87×10^{-7}	-8.36×10^{-14}
n	-8.17×10^{-5}	4.04×10^{-9}	
o	1.05×10^{-6}		

(i.e., H_2O, CO_2, and O_2), as well as the char properties, porosity ε_p, particle thickness e_p and reaction pre-exponential factor A_i, by three functions that take the form[34]

$$\log_{10}\omega_i = f\left(T, P_j, e_p, \varepsilon_p, A_i\right) \quad (18)$$

The functions of the char particle conversion rates in the three reactant gases are given in Eqs. 19–21, and the coefficient values are listed in Table 3.

Combustion function

$$\log_{10}\omega_1 = a + bT + cP_{O_2} + de_p + e\varepsilon_p + fA_{O_2} + gT^2$$
$$+ hP_{O_2}{}^2 + ie_p{}^2 + j\varepsilon_p{}^2 + kTP_{O_2} + lTe_p + mTA_{O_2} \quad (19)$$

Boudouard function

$$\log_{10}\omega_2 = a + bT + cP_{CO_2} + de_p + e\varepsilon_p + fA_{CO_2} + gT^2 + hP_{CO_2}{}^2$$
$$+ iTe_p + jT\varepsilon_p + kTA_{CO_2} + le_p\varepsilon_p + me_pA_{CO_2} + n\varepsilon_pA_{CO_2} \quad (20)$$

Steam gasification function

$$\log_{10}\omega_3 = a + bT + cP_{H_2O} + de_p + e\varepsilon_p + fA_{H_2O} + gT^2$$
$$+ hP_{H_2O}{}^2 + iTe_p + jT\varepsilon_p + kTA_{H_2O} + lP_{H_2O}A_{H_2O} \quad (21)$$
$$+ me_p\varepsilon_p + ne_pA_{H_2O} + o\varepsilon_pA_{H_2O}$$

The properties of wood char used in this model are $e_p = 5.5 \times 10^{-3}$m, $\varepsilon_p = 0.75$ and the pre-exponential factors are $A_{(O_2)} = 1.1 \cdot 10^9 \text{s}^{-1}\text{atm}^{-0.6}$, $A_{CO_2} = 1.2 \cdot 10^8 \text{s}^{-1}\text{atm}^{-0.7}$, and $A_{H_2O} = 3.55 \cdot 10^3 \text{s}^{-1}\text{atm}^{-0.8}$, respectively.

For the water–gas shift reaction (WGS), we used a simple reversible rate expression for CO conversion which was proposed by Moe[35]

$$v_4 = k_{WGS}P_{CO}P_{H_2O}\left(1 - \frac{P_{CO_2}P_{H_2}}{K_{eq}{}^{WGS}P_{CO}P_{H_2O}}\right)M_{CO} \quad (22)$$

$$k_{WGS} = 1.85\times10^{-5}\exp\left(12.88 - \frac{1855.5}{T}\right) \quad (23)$$

$$K_{eq}{}^{WGS} = \exp\left(\frac{4577.8}{T} - 4.33\right) \quad (24)$$

where k_{WGS} (mol g^{-1} min^{-1}) and $K_{eq}{}^{WGS}$ are the rate constant and equilibrium rate constant respectively.

From the knowledge of the reaction rates v_i, $i = 1,\ldots4$, the production term r_j of chemical species j appearing in Eqs. 9 and 13 can be expressed by

$$r_j = \sum_{i=1}^{4} v_{ij} v_i \quad (25)$$

where v_{ij} denotes the (algebraic, positive for product, negative for reactants) stoichiometric coefficient of species j in reaction i. Table 4 details the expression for the production terms of the chemical species.

Energy Balance Equation. With the assumption of local thermal equilibrium between the gas and solid phases, the equation of energy conservation writes

$$\left(U_gC_gc_{p,g}M_g + U_cC_cc_{p,c}M_c\right)\nabla T = \nabla \cdot (\lambda_b\nabla T) + \dot{Q}_r + \dot{Q}_{loss} \quad (26)$$

where convective heat transfer is represented by the term on the left-hand side of Eq. 26 and conductive heat transfer by the first term of the right-hand side. The effective thermal conductivity λ_b in the porous media is evaluated by assuming that heat conduction in the solid and gas phase takes place in parallel which follows from the fifth assumption that no heat transfer occurs between the solid and gas phases[36]

$$\lambda_b = (1-\varepsilon)\lambda_c + \varepsilon\lambda_g \quad (27)$$

Table 5 details the expression of the thermal conductivities of the chemical species in the two phases as a function of temperature.

In Equation 26, $\dot{Q}$ is the heat source term which can be expressed in function of the heats $\Delta H_{r,i}$ of reactions (1)–(4)

$$Q_r = -\sum_{i=1}^{4} v_i\Delta H_{r,i} \quad (28)$$

Conversely, the heat lost to the surrounding by convection from the outer wall of the reactor Q_{loss}, was estimated to be 37.7 kWm^{-3} by Teixeira[31] which is determined from Newton's law of cooling as

$$Q_{loss} = \frac{hA(T_w - T_\infty)}{V} \quad (29)$$

where A and V denote the outer surface area and volume of the reactor, respectively. The average wall temperature T_w and ambient temperature T_∞ were experimentally found to be 62°C and 20°C, respectively, and the heat transfer coefficient h is 10 Wm^{-2}K^{-1}.

Boundary Conditions. The system of differential equations formed by Eqs. 5–26 can be solved with the following set of boundary conditions that specify concentration, temperature and pressure values or their derivatives at the inlet ($z = 0$) and outlet ($z = H$) of the char bed:
- Concentration of species in gas and solid phases

$$\text{Inlet} \quad C_j|_{z=0} = C_{j,0} \quad (30)$$

Table 4. Expression for Production Term of Each Chemical Species

Chemical Species j	Expression for Production Term
r_C	$C_{c,0}[-\omega_1 - \omega_2 - \omega_3]$
r_{CO_2}	$C_{c,0}[\omega_1 - \omega_2] + v_4$
r_{H_2O}	$-C_{c,0}\omega_3 - v_4$
r_{O_2}	$-C_{c,0}\omega_1$
r_{CO}	$C_{c,0}[2\omega_2 + \omega_3] - v_4$
r_{H_2}	$C_{c,0}\omega_3 + v_4$

Table 5. Expression of the Thermal Conductivity of Gaseous Species and Char as a Function of Temperature

Species j	Thermal Conductivity (mW/m/K)	Temperature Range (K)	Refs.
N_2	$-0.3721 + 0.10977 \cdot T - 9.42549 \cdot 10^{-5} \cdot T^2 + 8.05548 \cdot 10^{-8} \cdot T^3 - 3.35367 \cdot 10^{-11} \cdot T^4 + 5.15605 \cdot 10^{-15} \cdot T^5$	65–2500	37
O_2	$-1.7536 + 0.1224 \cdot T - 1.322444 \cdot 10^{-4} \cdot T^2 + 1.7804 \cdot 10^{-7} \cdot T^3 - 1.200176 \cdot 10^{-10} \cdot T^4 + 2.9817302 \cdot 10^{-14} \cdot T^5$	70–1500	37
CO_2	$-0.341914 + 0.0314 \cdot T + 1.170458 \cdot 10^{-4} \cdot T^2 - 1.281 \cdot 10^{-7} \cdot T^3 + 5.7923 \cdot 10^{-11} \cdot T^4 - 9.72044 \cdot 10^{-15} \cdot T^5$	190–2000	37
H_2	$-4.0803 + 0.9858 \cdot T - 1.330466 \cdot 10^{-3} \cdot T^2 + 1.1217 \cdot 10^{-6} \cdot T^3 - 3.25582 \cdot 10^{-10} \cdot T^4$	16–1500	37
CO	$-0.42832 + 0.09941 \cdot T - 5.96573 \cdot 10^{-5} \cdot T^2 + 3.81583 \cdot 10^{-8} \cdot T^3 - 1.43131 \cdot 10^{-11} \cdot T^4 + 2.56748 \cdot 10^{-15} \cdot T^5$	80–2200	37
H_2O	148	1500	37
C	95.8	307	38

$$\text{Outlet} \quad n \cdot \nabla C_j|_{z=H} = 0 \qquad (31)$$

- Bed temperature

$$\text{Inlet} \quad T|_{z=0} = T_0 \qquad (32)$$

$$\text{Outlet} \quad n \cdot \nabla T|_{z=H} = 0 \qquad (33)$$

- Bed pressure

$$\text{Inlet} \quad -\frac{K}{\mu} \cdot \nabla P|_{z=0} = U_{g,0} \qquad (34)$$

$$\text{Outlet} \quad P|_{z=H} = P_{\text{atm}} \qquad (35)$$

OpenFOAM simulation

The system of partial differential equations discussed in the previous section was solved using the finite volume discretization method employed by OpenFOAM. The chemical and thermal properties data were obtained from *NIST-JANAF Thermochemical Tables*[39] and Teixeira.[31] A mesh convergence study was performed and an optimum value of 325 cells was found.

Results and Discussion
Validation of simulation model

The model predictions have been validated against three different sets of experimental results: two different feedstocks with the same operating conditions (Table 6), and two different experimental conditions with the same feedstock (Table 7). The results are presented in Table 8. It can be seen that the model predictions are in good agreement with all three experimental observations. Discrepancies remain regarding CO and H_2 concentrations at the outlet of the bed; nevertheless the model captures the trend well.

A more detailed evaluation of the model's ability to predict the evolution of the bed behavior along the bed height was made by comparing the predicted results with the experimental ones for char chip gasification provided by Teixeira et al.[24] The results are displayed in Figure 2 which reveal a highly reactive zone at the top of the bed ($z < 10$ cm) where the bed temperature decreases sharply to 875°C due to the predominant endothermic char gasification reactions involving H_2O and CO_2. Below this zone, the low temperatures slow down the char gasification reactions which in turn decrease the production of H_2 and CO. To estimate the accuracy of our simulation results (w_{is}) with respect to the experimental data (w_ie), the sum squared method was used

$$\text{Mean error}(\%) = 100 \sqrt{\frac{\sum_{i=1}^{N} \left(\frac{w_{ie} - w_{is}}{w_{ie}} \right)^2}{N}} \qquad (36)$$

The error analysis on our simulation results reveals a discrepancy of 4% for char conversion, 2% for bed temperature, 11% for H_2 and 4% for CO. These discrepancies are satisfactory given that the estimated experimental error reported by Teixeira et al.[24] is 11%.

Figure 2 also shows a discrepancy between our simulation results and those of Teixeira, especially on the concentration fields of H_2 and CO (Figures 2c, d). It appears that the improved prediction of CO concentration by our model may be linked to our choice of WGS kinetics (Eqs. 22–24), which differs from the one adopted by Teixeira and coworkers. The WGS kinetics used by Teixeira et al.[41] was for an uncatalyzed reaction (Eq. 37 and Table 9)

Table 6. Composition and Properties of Char from Maritime Pine Wood Chips and Pellets

	Van de Steene et al.,[40] Char Chips	Teixeira et al.,[24,33] Char Chips	Teixeira et al.,[33] Char Pellets
Proximate analysis (wt % dry basis)			
Ash	1.4	1.7	1.4
Volatile Matter	4.9	4.0	2.0
Fixed carbon (by difference)	93.7	94.3	96.6
Ultimate analysis (wt % dry basis)			
C	89.8	92.6	92.8
H	2.2	1.0	1.3
N	0.1	0.2	0.3
O	6.1	3.8	3.1
S	0.001	<0.2	>0.2
LHV (MJ kg^{-1} dry basis)	–[a]	33.4	33.1
Char bed bulk density (g cm^{-3})	–[a]	0.13	0.37
Particle density (g cm^{-3})	–[a]	0.33	0.66
Particle porosity (–)	–[a]	0.74	0.51
Particle average thickness (mm)	–[a]	5.2	4.2

[a]Value not provided by the author and hence is estimated to be the same as that for char chips used by Teixeira.

Table 7. Operating Conditions at the Bed Inlet for Char Gasification Experiments

Parameters	Van de Steene et al.,[40] Char Chips	Teixeira et al.,[24,33] Char Chips and Pellets
Gas (%; mol/min)		
H_2O	19; 2.35	28; 3.2
CO_2	9; 1.12	8.2; 0.9
O_2	2; 0.25	2.7; 0.3
N_2	59; 7.31	61.1; 7.0
CO	4; 0.5	0
H_2	7; 0.87	0
Solid char (g/min)	28	28
Temperature (°C)	950	1028
Total pressure (atm)	1.01	1
Gas velocity (m/s)	0.68	0.7
Bed height (cm)	65	65

$$v_4 = \frac{k_{WGS}}{(RT)^2}\left(P_{CO}P_{H_2O} - \frac{P_{CO_2}P_{H_2}}{K_{eq}^{WGS}}\right) \qquad (37)$$

where k_{WGS} and K_{eq}^{WGS} follow Arrhenius laws (Table 9).

On the contrary, our model uses Moe's kinetics[35] which accounts for WGS catalysis by iron oxide (Fe_2O_3) in the reactor bed. This choice is based on the knowledge that wood char contains ash which is composed of up to 9.5 wt % Fe_2O_3[42] and that commercially available high temperature WGS catalysts are typically manufactured from Fe_2O_3.[43] In the reactor entrance zone of 10 cm height where 80% of the char is converted to gas (Figure 2a), the remaining solid is essentially ash. Thus we expect that in this zone, the ash containing Fe_2O_3 will catalyze the WGS reaction and thus increase CO conversion. Although our use of Moe's WGS kinetics[35] significantly improved CO prediction (Figure 2d), the opposite held for H_2 (Figure 2c). This discrepancy for H_2 can be explained

Table 8. Experimental and Predicted Results for Char Bed Outlet Conditions

	Van de Steene et al.,[40] Char Chips		Teixeira et al.,[24,33] Char Chips		Teixeira et al.,[33] Char Pellets	
	Exp.	Num.	Exp.	Num.	Exp.	Num.
T (°C)	700	688	770	731	730	692
H_2O (vol %)	9.8	8.2	11.5	11.2	11.5	9.5
CO_2 (vol %)	10.8	10.2	10.0	11.0	9.0	11.1
O_2 (vol %)	0.6	0.0	0.0	0.0	0.0	0.0
H_2 (vol %)	15.9	15.5	14.0	13.4	13.5	14.8
CO (vol %)	9.8	12.4	11.2	10.5	11.5	11.4
N_2 (vol %)	52.9	53.7	53.3	53.9	54.6	53.1
Solid char (g/min)	3.1	3.6	~2.5[a]	2.3	~2.8[b]	2.9
Char conversion, X	89	71	95	87	95.0	99.0

[a]Calculated at a bed height of 50 cm.
[b]Calculated at a bed height of 15 cm.

from the observation that in Figures 2c, and 2d, close to the reactor exit, H_2 is still being produced while CO is consumed. This is because the WGS reaction rate does not reach equilibrium as shown in Figure 3 by the positive value of the reaction rate at the reactor exit. Hence, given a longer reactor, we expect that the error observed for H_2 will diminish as the WGS reaction nears equilibrium. Nonetheless, it is clear that the choice of the WGS kinetics plays a key role in predicting the final syngas composition.

Sensitivity analysis

The aim of this analysis is to investigate the influence of the bed inlet temperature on the one hand, and of the gas composition on the other hand, on the bed temperature profile T, char
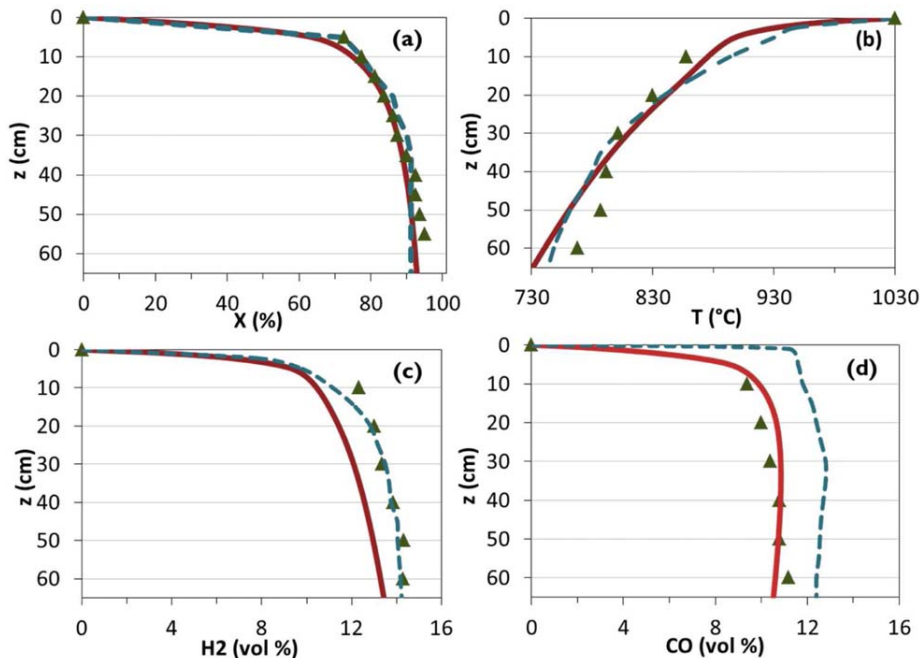

Figure 2. Experimental and numerical results for char conversion (a), temperature profile (b), H_2 concentration (c) and CO concentration (d).

In all graphs, the experimental data provided by Teixeira et al.[24] are represented by triangles, and the predicted values from OPENFOAM and COMSOL[24] simulations are represented by solid and dashed lines, respectively. [Color figure can be viewed in the online issue, which is available at wileyonlinelibrary.com.]

conversion X and syngas composition (CO, H_2). Char from maritime pine wood chips is the chosen feedstock whose composition and properties are provided by Teixeira et al.[24,33] and are shown in Table 6. The operating conditions used for this study are displayed in Table 10.

To perform the sensitivity analysis, the following operating parameters were varied:
- Inlet bed temperature, T_0: 900–1000 °C
- O_2 concentration, $C_{O_2,0}$: 0–3 vol %
- Steam concentration, $C_{H_2O,0}$: 5–20 vol %
- CO_2 concentration, $C_{CO_2,0}$: 5–20 vol %

For each set of operating parameters, their influence is investigated by analyzing the char conversion, bed temperature profile and the production of H_2 and CO along the char bed. Moreover the evolution of the different reaction rates is examined to clarify the mechanism involved.

Effect of Inlet Bed Temperature. Figure 4 shows the simulation results for char conversion, temperature profile, H_2 and CO concentration for different inlet bed temperatures. These results show that an increase in the bed inlet temperature from 900 to 1000 °C increases overall char conversion and CO concentration by 27 % and 33 % respectively. It also increases to a lesser extent the concentration of H_2 and outlet temperature (17% and 14°C, respectively). Consequently, the H_2/CO ratio decreases from 0.7 to 0.6. These results can be explained by observing the influence of inlet bed temperature on the reaction rates as shown in Figure 5. Figures 5a and 5b, show that in the 5 cm entrance zone of the reactor, the increase in bed temperature causes a drastic rise of the endothermic steam gasification and Boudouard reactions (Eqs. 2 and 3). This leads to a strong increase in CO production and an insignificant rise in H_2 production. Higher temperatures in this reaction zone also favor the production of CO to the detriment of H_2 by shifting the WGS equilibrium position to the left (Eq. 4). This effect of inlet bed temperature on CO enrichment in syngas is consistent with the observations made by Yang et al.[11] from char gasification experiments at lower temperatures
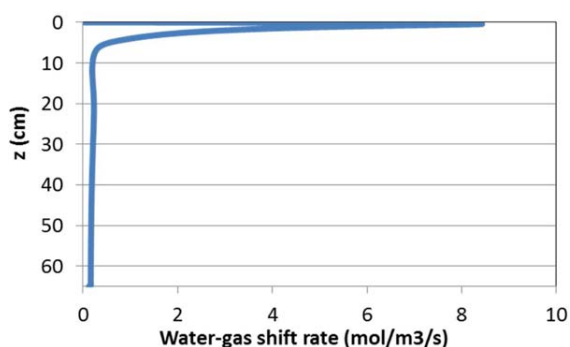

Figure 3. Evolution of WGS reaction rate along the char bed at the operating conditions specified in Table 6.

[Color figure can be viewed in the online issue, which is available at wileyonlinelibrary.com.]

(500–800 °C). Producing CO-rich syngas (low H_2/CO ratio) is desirable for FT synthesis. However this may not justify the indirect heating of the reactor to temperatures above 900 °C due to the associated high energy costs and the relatively small gain in lowering in the H_2/CO ratio.

Effect of O_2 Concentration. The simulation results for char conversion, temperature profile, H_2 and CO concentration for different O_2 concentration of the inlet gas stream are shown in Figure 6. The results show that an increase in O_2 concentration from 0 to 3 vol % increases the overall char conversion by 48%, the bed outlet temperature by 86 °C and the production of H_2 and CO by 20 % and 133 % respectively. Thus the H_2/CO ratio falls from 0.8 to 0.4. To understand this phenomenon, it is useful to examine the evolution of the different reaction rates (Figure 7). In an entrance zone of 10 cm height, the increase in O_2 concentration strongly increases the combustion rate which produces more CO_2 and raises the bed temperature (Eq. 1). The production of CO_2 favors in turn the Boudouard reaction and thus more CO is produced (Eq. 2). Next, the combination of CO_2 and bed temperature increase shifts the WGS equilibrium to the left which increases production of H_2O (Eq. 4) and further increases production of CO. Finally, the steam gasification reaction (Eq. 3) is favored by the increase of H_2O and thus also contributes to the production of CO and H_2. Hence the simulation results show that a relatively small increase in O_2 concentration (0–3 vol %) strongly increases char conversion to favor CO production and also increases bed temperatures. Yang et al.[12] have reported a similar effect of O_2 in air on CO production and bed temperature when air velocity is increased during char gasification. Thus our results show that raising the O_2 concentration is beneficial to provide direct heating to the reactor and to produce syngas with a low H_2/CO ratio for FT synthesis. Of course, a trade-off must be found between this benefit of increasing O_2 and the additional costs incurred from operating at higher air flow rates or producing oxygen-enriched air from air separating units.

Effect of H_2O Concentration. Figure 8 shows the numerical results for char conversion, temperature profile, H_2 and CO concentration for different H_2O concentrations of the inlet gas stream. It can be seen that the increase in H_2O concentration from 5 to 20 vol % raises the overall char conversion by 17 % and the H_2 production by 150 %, whereas it decreases the CO production by 33 % and the bed outlet temperature by 6 °C. As a result, the H_2/CO ratio increases from 0.3 to 1.3. Figure 9 shows that in an entrance zone of 6 cm height, the increase in H_2O concentration boosts the steam gasification reaction (Eq. 3), thereby producing more CO and H_2. Much of this CO produced is consumed by the WGS reaction to favor H_2 production (Eq. 4). As steam gasification is an endothermic reaction, an increase in its reaction rate decreases the bed temperature

Table 10. Operating Conditions for Sensitivity Analysis

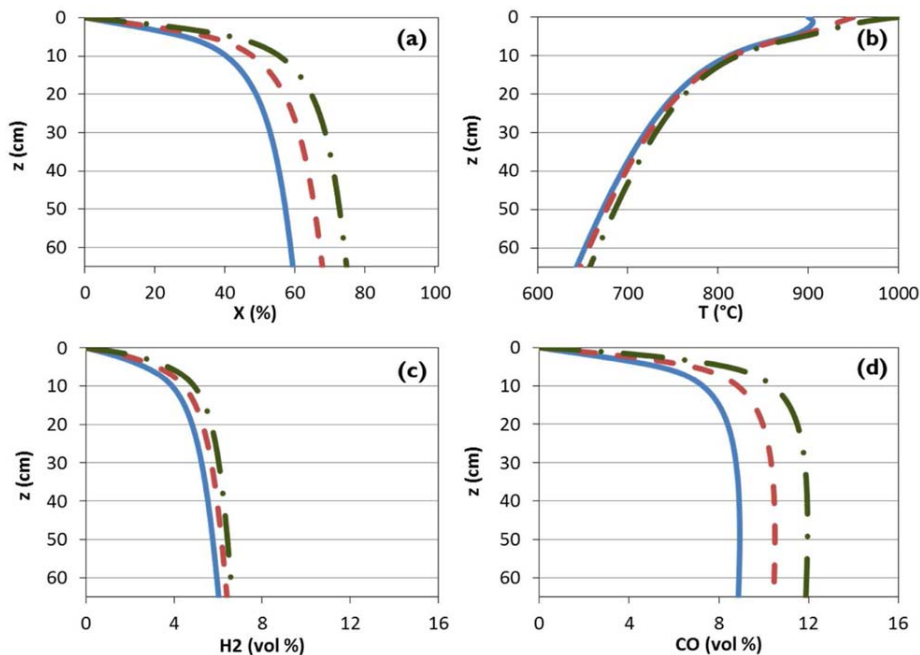| T (°C)	O_2 (vol %)	H_2O (vol %)	CO_2 (vol %)	N_2 (vol %)
900	1.5	10	10	78.5
1000	1.5	10	10	78.5
950	0.0	10	10	80.0
950	3.0	10	10	77.0
950	1.5	20	10	68.5
950	1.5	5	10	83.5
950	1.5	10	20	68.5
950	1.5	10	5	83.5

Figure 4. Influence of inlet temperature (900°C—solid line, 950°C—dashed line, 1000°C—dash-dotted line) on char conversion (a), temperature profile (b), H_2 concentration (c), and CO concentration (d).

[Color figure can be viewed in the online issue, which is available at wileyonlinelibrary.com.]

which in turn decreases the rate of the Boudouard reaction and the production of CO. Thus an increase in H_2O concentration in the gas at the bed inlet results in a significant increase in H_2 production to the detriment of CO production. Steam gasification experiments of biomass char in a fixed bed reactor by Yan et al.[13] have revealed that increasing steam flow rate from 0 to 0.165 g/min/g of biomass char increased H_2/CO ratio from 0.88 to 3.74. Consequently, syngas produced from steam gasi-

fication can be used in gas turbine combustion and Solid oxide fuel cells (SOFC).

Effect of CO_2 Concentration. Figure 10 shows the numerical results for char conversion, temperature profile, H_2 and CO concentration for different CO_2 concentrations of the inlet gas stream. The results reveal that the increase in CO_2 concentration from 5 to 20 vol % increases the overall char conversion by 74 %, the outlet bed temperature by 27 °C and the CO
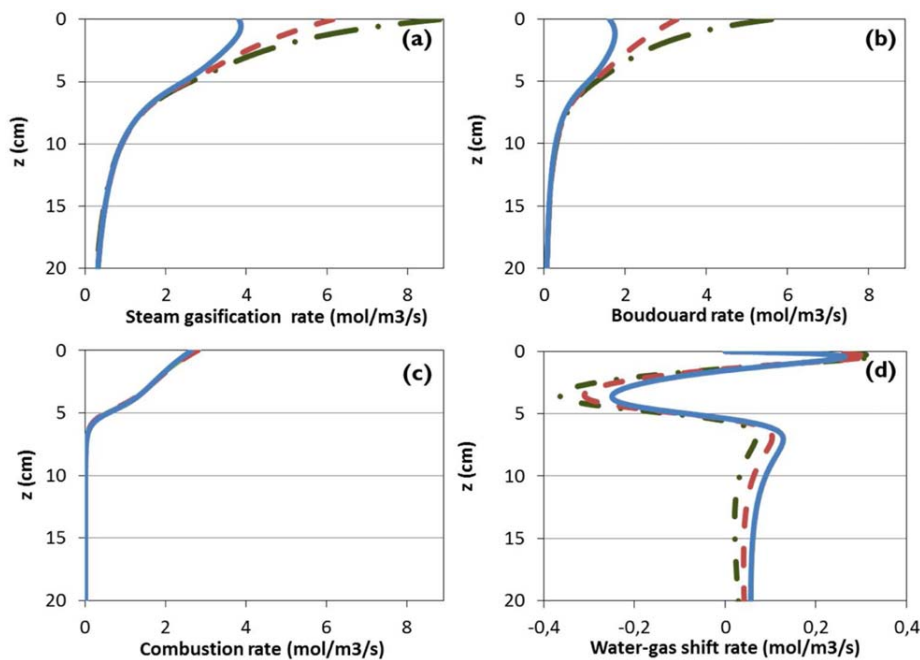

Figure 5. Influence of inlet temperature: (900 °C—solid line, 950 °C—dashed line, 1000 °C—dash-dotted line) on rates of steam gasification (a), Boudouard (b), combustion (c), and WGS (d).

[Color figure can be viewed in the online issue, which is available at wileyonlinelibrary.com.]
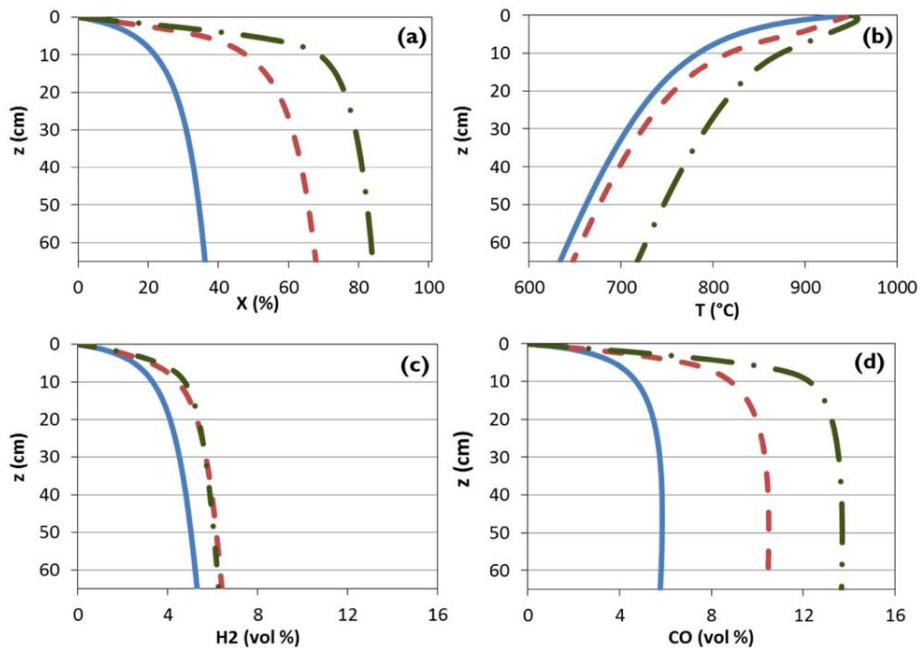
Figure 6. Influence of O_2 concentration (0 vol %—solid line, 1.5 vol %—dashed line, 3 vol %—dash-dotted line) on char conversion (a), temperature profile (b), H_2 concentration (c), and CO concentration (d).

[Color figure can be viewed in the online issue, which is available at wileyonlinelibrary.com.]

production by 10 %, whereas it decreases the H_2 production by 35 %. As a result, the H_2/CO ratio decreases from 0.7 to 0.4. Figure 11 shows that between the bed inlet and a height of 10 cm, the increase in CO_2 concentration from 5 to 10 vol % increases the Boudouard reaction rate and shifts the WGS equilibrium position to the left, thus it increases CO (8 %) and decreases H_2 (12 %). As both of these reactions are endother-

mic, the bed temperature decreases. However when the initial CO_2 is 20 vol %, the decrease in bed temperature is significant enough to decelerate the steam gasification reaction between the bed height of 10 cm and 20 cm from the inlet, as shown in Figure 11a. This decrease in the steam gasification rate not only decreases the CO and H_2 production as predicted by Eq. 3, but also increases the bed temperature as observed in
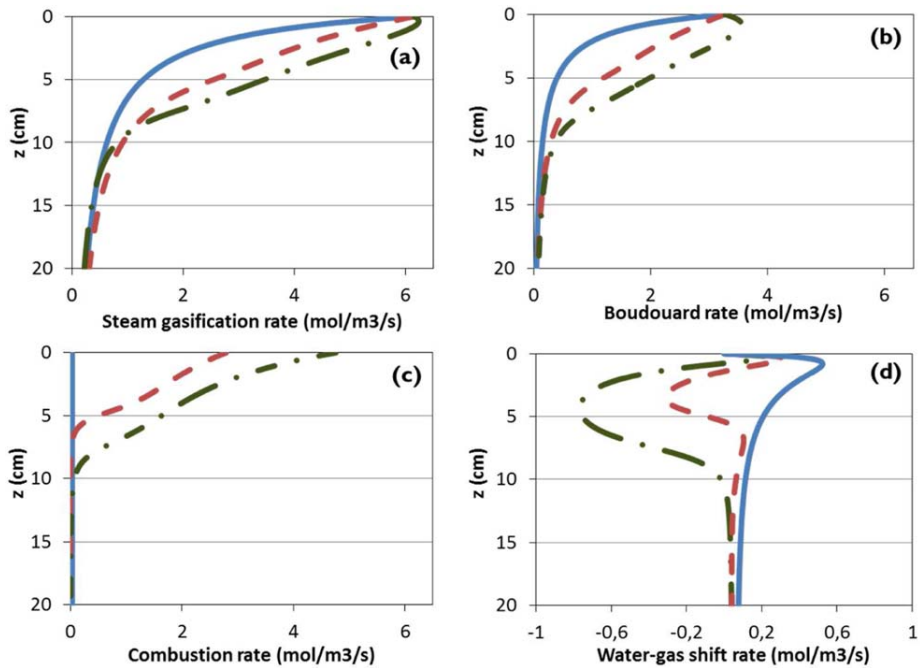

Figure 7. Influence of O_2 concentration (0 vol %—solid line, 1.5 vol %—dashed line, 3 vol %—dash-dotted line) on rates of steam gasification (a), Boudouard (b), combustion (c), and WGS (d).

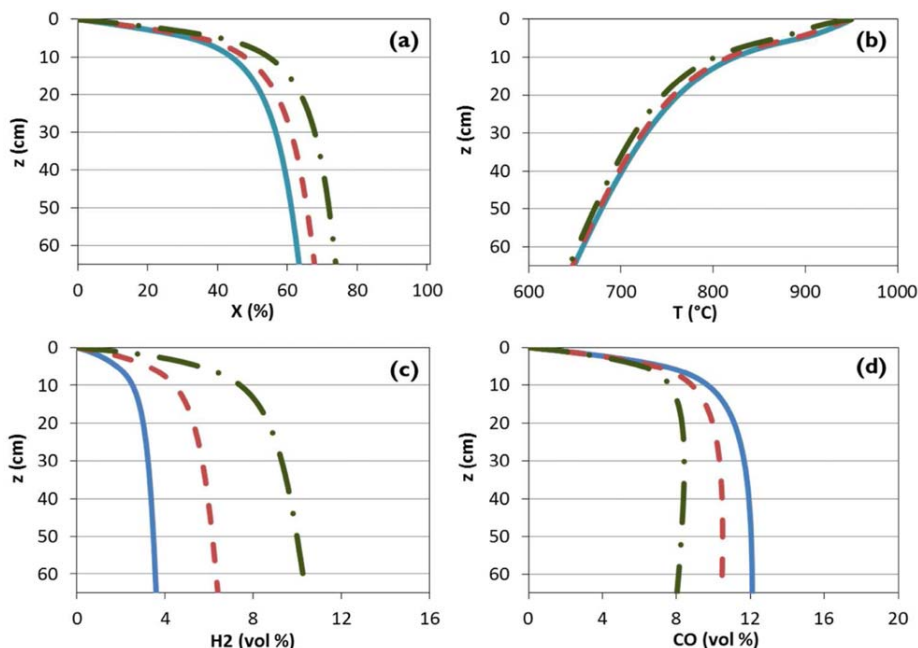[Color figure can be viewed in the online issue, which is available at wileyonlinelibrary.com.]

Figure 8. Influence of H_2O concentration (5 vol %—solid line, 10 vol %—dashed line, 20 vol %—dash-dotted line) on char conversion (a), temperature profile (b), H_2 concentration (c), and CO concentration (d).

[Color figure can be viewed in the online issue, which is available at wileyonlinelibrary.com.]

Figure 10b. Thus, although CO production is favored by the increase in the initial CO_2 concentration from 5 to 10 vol %, a further increase in the latter from 10 to 20 vol % actually lowers the syngas quality, because the net increase of CO is insignificant (2 %) and H_2 production is further decreased by 27 %. These results are consistent with the experimental results of Butterman and Castaldi[6] who observed that introducing 0 to 5 vol % CO_2 during biomass gasification, increased CO by a factor of 10 and decreased H_2 by a factor of 3.3 at 900 °C. However increasing CO_2 from 5 to 50 vol % resulted in CO increases and H_2 decreases by a factor of 3. Thus in view of recycling large streams of CO_2 produced from industrial processes, our results show that low concentrations of CO_2 should be used if CO_2 were to serve as a gasifying agent for controlling syngas composition.
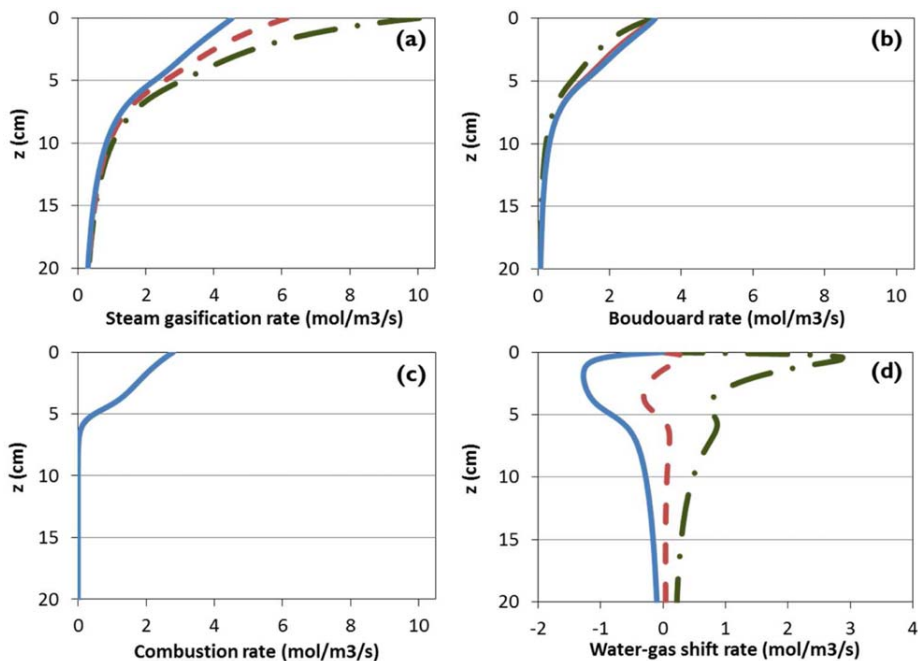

Figure 9. Influence of H_2O concentration (5 vol %—solid line, 10 vol %—dashed line, 20 vol %—dash-dotted line) on rates of steam gasification (a), Boudouard (b), combustion (c), and WGS (d).

[Color figure can be viewed in the online issue, which is available at wileyonlinelibrary.com.]
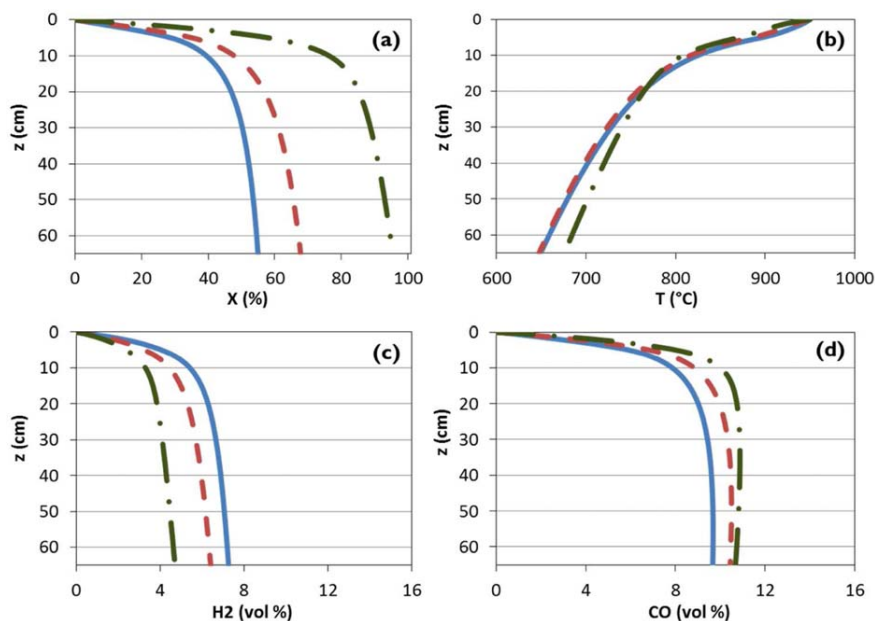
Figure 10. Influence of CO_2 concentration (5 vol %—solid line, 10 vol %—dashed line, 20 vol %—dash-dotted line) on char conversion (a), temperature profile (b), H_2 concentration (c), and CO concentration (d).

[Color figure can be viewed in the online issue, which is available at wileyonlinelibrary.com.]

Figure 11. Influence of CO_2 concentration (5 vol %—solid line, 10 vol %—dashed line, 20 vol %—dash-dotted line) on rates of steam gasification (a), Boudouard (b), combustion (c), and WGS (d).

[Color figure can be viewed in the online issue, which is available at wileyonlinelibrary.com.]
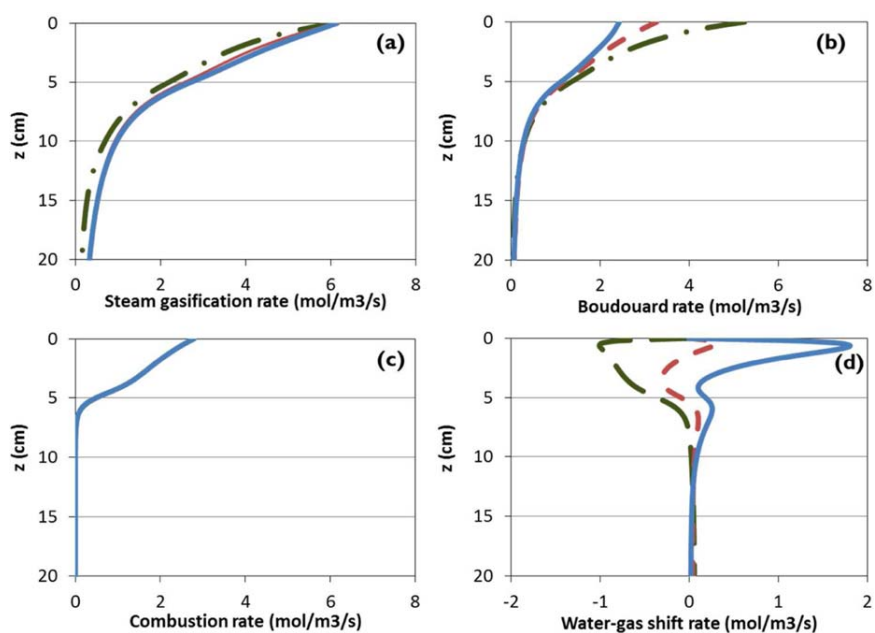
Table 11. Summary of Simulation Results from Sensitivity Analysis

	Char conversion, X (%)	Temperature, T (°C)	H_2 (vol %)	CO (vol %)	$H_2/$ CO
T (900–1000 °C)	+27%	+14	+17%	+33%	−0.1
O_2 (0–3 vol %)	+48%	+86	+20%	+133%	−0.4
H_2O (5–20 vol %)	+17%	−6	+150%	−33%	+1.0
CO_2 (5–10 vol %)	+23%	−1.7	−12%	+8%	−0.1
CO_2 (10–20 vol %)	+41%	+28	−27%	+2%	−0.2

Conclusions

In this article, a 1-D CFD simulation model developed using OpenFOAM was presented to simulate the gasification of wood char in a downdraft reactor. Good quantitative agreement between the numerical results of the simulation and published experimental data was achieved. A sensitivity analysis was also conducted to investigate the influence of the bed inlet temperature and the inlet gas composition on char conversion, temperature profile and concentrations of CO and H_2 in the product gas. A summary of the results obtained from the sensitivity analysis is shown in Table 11. From these results, the following conclusions can be drawn:

- A rise in inlet bed temperatures above 900 °C has a relatively small influence on char conversion and syngas H_2/CO ratio.
- O_2 and H_2O have the strongest influence on syngas CO and H_2 concentrations respectively. A small increase in O_2 concentration from 0 to 3 vol % increases char conversion and bed temperature to produce a syngas rich in CO (low H_2/CO ratio) and thus suitable for FT synthesis. An increase in H_2O concentration from 5 to 20 vol % results in a significant increase in H_2 (high H_2/CO ratio) and thus favors the production of syngas for use in gas turbines and solid oxide fuel cells (SOFC).
- Although increasing the inlet CO_2 concentration from 5 to 10 vol % increases the char conversion and CO production, further increasing the inlet CO_2 concentration from 10 to 20 vol % actually lowers the syngas quality because the net increase of CO is small and H_2 production is further decreased. This restricts the recycling of industrial CO_2 as an agent for controlling syngas composition.

The in-house built OpenFOAM solver used in this work is the first of its kind to simulate the gasification of biomass at the reactor scale in a downdraft gasifier. The development of this simulation model which is capable of predicting the composition of syngas with varying operating conditions provides essential knowledge for optimizing the design and operation of downdraft gasifiers.

Future Work

The model presented in this article can be modified to simulate the gasification of raw biomass in a stratified downdraft reactor. To do so, submodels describing the drying and pyrolysis stages of the gasification processes could be incorporated. Furthermore, as a result of the low computation time for each simulation run (30 s average), optimization techniques can be used to determine optimal reactor design and operating conditions with respect to the syngas H_2/CO ratio desired.

Acknowledgments

Notation

A = pre-exponential factor, s^{-1}
C = molar concentration, mol/m^3
c_p = specific heat capacity, J/g·K
D = diffusion coefficient, m^2/s
e_p = char particle thickness, m
Δh = heat of reaction, J/mol
K = permeability, m^2
k_{WGS} = rate constant for water gas shift reaction, $m^3/mol·s$
K_{eq}^{WGS} = equilibrium rate constant for water gas shift reaction, –
M = molar mass, g/mol
$\dot{n}$ = molar flow rate, mol/s
P = pressure, Pa
$\dot{Q}$ = heat source, W/m^3
r = reaction rate, mol/m^3 s
R = universal gas constant, = 8.314 J/mol·K
T = temperature, K
U = velocity, m/s
X = char conversion, –

Greek letters

ε = porosity
λ = thermal conductivity, W/m·K
μ = dynamic viscosity, kg/m·s

Subscripts

b = porous char bed
c = solid char phase
e = experimental
g = gas phase
i = ith reaction
j = jth gas species
p = char particle
s = simulated
0 = initial

Literature Cited

1. IEO. *International Energy Oulook: 2013*. 2013. http://www.eia.gov/forecasts/ieo/pdf/0484%282013%29.pdf.
2. Van Der Drift A, van Ree R, Boerrigter H. Bio-syngas: key intermediate for large scale production of green fuels and chemicals. *2nd World Conf Technol Exhib Biomass Energy Ind Clim Prot*. 2004:88. https://www.ecn.nl/publications/PdfFetch.aspx?nr=ECN-RX–04-029#page=88.
3. Alakangas E, Valtanen J, Levlin J. CEN technical specification for solid biofuels—fuel specification and classes. *Biomass Bioenergy*. 2006;30(11):908–914.
4. Boerrigter H, Rauch R. Syngas production and utilisation. In: Knoef HA., ed. *Handbook Biomass Gasification*. Biomass Technology Group (BTG); 2005.
5. Basu P. *Biomass Gasification and Pyrolysis: Practical Design and Theory*. Burlington, MA: Academic Press, 2010.
6. Butterman HC, Castaldi MJ. CO2 as a carbon neutral fuel source via enhanced biomass gasification. *Environ Sci Technol*. 2009;43(23):9030–9037.
7. Arena U. Process and technological aspects of municipal solid waste gasification. A review. *Waste Manage*. 2012;32(4):625–639.
8. Belgiorno V, De Feo G, Della Rocca C, Napoli RMA. Energy from gasification of solid wastes. *Waste Manage*. 2003;23(1):1–15.
9. Devi L, Ptasinski KJ, Janssen FJJG. A review of the primary measured for tar elimination in biomass gasification processes. *Biomass Bioenergy*. 2003;24:125–140.
10. Klaas M, Greenhalf C, Ferrante L, Briens C, Berruti F. Optimisation of hydrogen production by steam reforming of chars derived from lumber and agricultural residues. *Int J Hydrog Energy*. 2015;40(9):3642–3647.
11. Yang C, Jia L, Su S, Tian Z, Song Q, Fang W, Chen C, Liu G. Utilization of CO2 and biomass char derived from pyrolysis of Dunaliella salina: the effects of steam and catalyst on CO and H2 gas production. *Bioresour Technol*. 2012;110:676–681.
12. Yang YB, Ryu C, Sharifi VN, Swithenbank J. Effect of model and operating parameters on air gasification of char. *Energy Fuels*. 2006;20(4):1698–1708.
13. Yan F, Luo S, Hu Z, Xiao B, Cheng G. Hydrogen-rich gas production by steam gasification of char from biomass fast pyrolysis in a fixed-bed reactor: influence of temperature and steam on hydrogen yield and syngas composition. *Bioresour Technol*. 2010;101(14):5633–5637.
14. Chaudhari ST, Bej SK, Bakhshi NN, Dalai AK. Steam Gasification of biomass-derived char for the production of carbon monoxide-rich synthesis gas. *Energy Fuels*. 2001;15(3):736–742.

15. Moazami N, Wyszynski ML, Mahmoudi H, Tsolakis A, Zou Z, Panahifar P, Rahbar K. Modelling of a fixed bed reactor for Fischer–Tropsch synthesis of simulated N2-rich syngas over Co/SiO2: hydrocarbon production. *Fuel*. 2015;154:140–151.
16. Hamel S, Krumm W. Mathematical modelling and simulation of bubbling fluidised bed gasifiers. *Powder Technol*. 2001;120(1–2): 105–112.
17. Ahmed TY, Ahmad MM, Yusup S, Inayat A, Khan Z. Mathematical and computational approaches for design of biomass gasification for hydrogen production: a review. *Renew Sustain Energy Rev*. 2012; 16(4):2304–2315.
18. Koenig PC, Squires RG, Laurendeau NM. Evidence for two-site model of char gasification by carbon dioxide. *Carbon*. 1985;23(5): 531–536.
19. Guizani C, Escudero Sanz FJ, Salvador S. Influence of temperature and particle size on the single and mixed atmosphere gasification of biomass char with H2O and CO2. *Fuel Process Technol*. 2015;134: 175–188.
20. Fermoso J, Gil MV, Pevida C, Pis JJ, Rubiera F. Kinetic models comparison for non-isothermal steam gasification of coal–biomass blend chars. *Chem Eng J*. 2010;161(1–2):276–284.
21. Kramb J, Konttinen J, Gómez-Barea A, Moilanen A, Umeki K. Modeling biomass char gasification kinetics for improving prediction of carbon conversion in a fluidized bed gasifier. *Fuel*. 2014;132:107–115.
22. Septien S, Escudero Sanz FJ, Salvador S, Valin S. Steam gasification of char from wood chips fast pyrolysis: development of a semi-empirical model for a fluidized bed reactor application. *Biomass Bioenergy*. 2015;77:64–74.
23. Wang Y, Yan L. CFD studies on biomass thermochemical conversion. *Int J Mol Sci*. 2008;9(6):1108–1130.
24. Teixeira G, Van de Steene L, Salvador S, Gelix F, Dirion J-L, Paviet F. Gasification of continuous wood char bed: modelling and experimental approach. *Chem Eng Trans*. 2014;37:247–252.
25. Kwiatkowski K, Zuk PJ, Dudyński M, Bajer K. Pyrolysis and gasification of single biomass particle—new openFoam solver. *J Phys Conf Ser*. 2014;530:012015.
26. Van de steene L, Tagutchou JP, Escudero Sanz FJ, Salvador S. Gasification of woodchip particles: experimental and numerical study of char–H2O, char–CO2, and char–O2 reactions. *Chem Eng Sci*. 2011; 66(20):4499–4509.
27. Lamarche P, Tazerout M, Gelix F, Köhler S, Mati K, Paviet F. Modelling of an indirectly heated fixed bed pyrolysis reactor of wood: transition from batch to continuous staged gasification. *Fuel*. 2013; 106:118–128.
28. Anca-Couce A, Berger A, Zobel N. How to determine consistent biomass pyrolysis kinetics in a parallel reaction scheme. *Fuel*. 2014; 123:230–240.
29. Vijeu R, Gerun L, Tazerout M, Castelain C, Bellettre J. Dimensional modelling of wood pyrolysis using a nodal approach. *Fuel*. 2008; 87(15–16):3292–3303.
30. Gomezbarea A, Ollero P, Arjona R. Reaction-diffusion model of TGA gasification experiments for estimating diffusional effects. *Fuel*. 2005;84:1695–1704.
31. Teixeira G. *Gazéification de charbon de granules de bois: comportement thermochimique et mécanique d'un lit fixe continu [dissertation]*. Institut National Polytechnique de Toulouse, France. 2012. http://oatao.univ-toulouse.fr/6986/.
32. Comiti J, Renaud M. A new model for determining mean structure parameters of fixed beds from pressure drop measurements: application to beds packed with parallelepipedal particles. *Chem Eng Sci*. 1989;44(7):1539–1545.
33. Teixeira G, Van de Steene L, Martin E, Gelix F, Salvador S. Gasification of char from wood pellets and from wood chips: textural properties and thermochemical conversion along a continuous fixed bed. *Fuel*. 2012;102:514–524.
34. Teixeira G, Van de steene L, Ponthieux A, Salvador S. Prediction of the gasification kinetics of a single wood char particle from a limited set of parameters. *Fuel*. 2014;123:194–204.
35. Moe JM. Design of water-gas shift reactors. *Chem Eng Prog*. 1962; 58(3):33.
36. Nield DA, Bejan A. Heat transfer through a porous medium. In: *Convection in Porous Media*. New York, NY: Springer New York; 2013:31–46. Available at: http://link.springer.com/10.1007/978-1-4614-5541-7_2. Accessed on August 28, 2015.
37. Le Neindre B. Mesure de la conductivité thermique des liquides et des gaz. *Tech Ing*. 1996;R2920:15–22. http://www.techniques-ingenieur.fr/res/pdf/encyclopedia/42544210-r2920.pdf.
38. Gupta M, Yang J, Roy C. Specific heat and thermal conductivity of softwood bark and softwood char particles⋆. *Fuel*. 2003;82(8): 919–927.
39. Chase MW, Jr. NIST-JANAF Themochemical Tables, Fourth Edition. *J Phys Chem Ref Data Monogr*.1998;9:1–1951.
40. Gururajan VS, Agarwal PK, Agnew JB. Mathematical modelling of fluidized bed coal gasifiers. *Chem Eng Res Des*. 1992;70a:211–238.
41. Vassilev SV, Baxter D, Vassileva CG. An overview of the behaviour of biomass during combustion: part I. Phase-mineral transformations of organic and inorganic matter. *Fuel*. 2013;112:391–449.
42. Smith RJ, Loganathan M, Shantha MS. A review of the water gas shift reaction kinetics. *Int J Chem React Eng*. 2010;8(1). http://www.degruyter.com/view/j/ijcre.2010.8.1/ijcre.2010.8.1.2238/ijcre.2010.8.1.2238.xml. Accessed March 18, 2015.
43. Van de steene L, Tagutchou JP, Mermoud F, Martin E, Salvador S. A new experimental continuous fixed bed reactor to characterise wood char gasification. *Fuel*. 2010;89(11):3320–3329.